Reduced Gravity Control of Small Spacecraft using Control Moment Gyroscopes and On-Off Thrusters

Todd F. Sheerin,[1] Jose Gomez, [2] Danilo Roascio, [3] and Jeffrey A. Hoffman[4]
Massachusetts Institute of Technology, Cambridge, MA 02139

Large spacecraft like the International Space Station have long benefited from the use of control moment gyroscopes (CMGs) as propellantless angular momentum devices, yet the large size of traditional CMGs generally prevent their application to small spacecraft platforms. Recent advances in the miniaturization of CMGs have motivated Draper and MIT to investigate the use of CMGs as attitude actuators for small spacecraft and for astronaut maneuvering units derived from NASA's SAFER system. On-off thrusters typical in reaction control systems produce fixed forces and torques over variable on-times, and pointing precision is limited by a deadband arising from minimum torque magnitude and duration. CMGs, by contrast, produce variable torques by gimbaling a fixed-rate flywheel; small gimbal rates correspond to small torques while large gimbal rates correspond to large torques. This wider range of torques can enable smaller deadbands (enhanced pointing precision) as well as improved slewing and disturbance rejection. When applied to small spacecraft with moving parts or to astronaut maneuvering systems, CMGs can provide stability without the use of fuel during dynamic operations that would not be possible with traditional thruster reaction control. Microgravity demonstration of thruster and CMG attitude control with the MIT Synchronized Position Hold, Engage, Reorient Experimental Satellites (SPHERES) facility and Honeybee Robotics miniature CMGs was recently conducted aboard NASA's Reduced Gravity Aircraft in August 2015 (Technology 138-P). CMG torques and SPHERES thruster torques on the same system were compared both in microgravity and in the laboratory. CMGs repeatedly generated both smaller and larger torques than thrusters alone could provide, indicating their capacity to improve control authority in the SPHERES system.

Nomenclature

$\hat{e}_i$	=	SPHERES body frame axis; *i* = *X*, *Y*, and *Z* are principal axes, *i* = XZ is in the $-(\hat{e}_X + \hat{e}_Z)/\sqrt{2}$ direction
$\vec{H}_{CMG}$	=	collective CMG angular momentum (N m s)
$\vec{h}_{CMG}$	=	individual CMG angular momentum (N m s), including flywheel and gimbal angular momenta
$\vec{h}_{fly}$	=	flywheel angular momentum (N m s) of an individual CMG rotor
I	=	mass moment of inertia (kg m^{-2}) tensor
I_{ij}	=	moment of inertia (kg m^{-2}) tensor element with respect to SPHERES axes $\hat{e}_i$ and $\hat{e}_j$
$\vec{F}_{thr}$	=	thrust force (N) of a SPHERES thruster
$\dot{m}$	=	mass flow rate (kg s^{-1})
$\vec{r}$	=	moment arm (m)
$\vec{L}_k$	=	SPHERES angular momentum (N m s) generated by an actuator indicated by subscript *k*
$\vec{v}_{prop}$	=	propellant velocity (m s^{-1})
T	=	torque actuation time (s)
ΔA	=	attitude control deadband width in angular acceleration space (rad s^{-2})
$\Delta\Theta$	=	attitude control deadband width in angular space (rad)
$\Delta\Omega$	=	attitude control deadband width in angular rate space (rad s^{-1})
ξ	=	thrust alignment angle (rad)

[1] Ph.D. Candidate, MIT Aeronautics and Astronautics, 70 Vassar St. 37-360, Cambridge MA 02139.
[2] Undergraduate, MIT Aeronautics and Astronautics.
[3] Postdoctoral Researcher, MIT Aeronautics and Astronautics.
[4] Professor of the Practice, MIT Aeronautics and Astronautics.

σ = standard deviation of data
$\vec{\tau}_{CMG\ total}$ = torque (N m) applied to a spacecraft from CMGs
$\vec{\tau}_i$ = torque (N m) applied to SPHERES satellite configuration about the SPHERES axis $\hat{e}_i$
$\vec{\tau}_{thr\ 1}$ = torque (N m) applied to a spacecraft from a single thruster
$\vec{\tau}_{thr}$ = torque (N m) applied to a spacecraft from a thruster pair
$\vec{\tau}_{s/c}$ = total torque (N m) applied to a spacecraft
ϕ = CMG gimbal angle (rad); for a scissor pair, gimbal angles are labeled ϕ_1 and ϕ_2 and $\phi = \phi_1 = -\phi_2$
$\dot{\phi}$ = CMG gimbal rate (rad s^{-1}); for a scissor pair, gimbal rates are labeled $\dot{\phi}_1$ and $\dot{\phi}_2$ and $\dot{\phi} = \dot{\phi}_1 = -\dot{\phi}_2$
$\vec{\omega}_i^{B/N}$ = angular rate (rad s^{-1}) about the SPHERES axis $\hat{e}_i$ measured from a fixed-SPHERES body reference frame *B* with respect to the laboratory inertial reference frame *N*
$\dot{\vec{\omega}}_i^{B/N}$ = angular acceleration (rad s^{-2}) about the SPHERES axis $\hat{e}_i$ measured from a fixed-SPHERES body reference frame *B* with respect to the laboratory inertial reference frame *N*

I. Introduction

FUTURE human and robotic space exploration and commercial space missions will require advanced capabilities to maneuver in low gravity environments. The use of control moment gyroscopes (CMGs) as internal momentum devices has traditionally been limited to large spacecraft given CMGs' commonly large size. Recent advances in CMG miniaturization, however, prompt their consideration in small spacecraft platforms. The Massachusetts Institute of Technology (MIT) and the Charles Stark Draper Laboratory, Inc. (Draper) have been investigating the use of CMGs as a means to augment thruster-based reaction control systems and improve platform stability. In recent years, the concept has been explored with respect to an astronaut maneuvering unit based on NASA's SAFER for low gravity extravehicular activities (EVAs) [1-5] as well as with respect to satellite inspection, servicing, and assembly applications [1, 6].

A. The Case for CMGs

The advantages of using CMGs as opposed to thrusters for reaction control is most prominently displayed at the International Space Station (ISS), which uses a set of four double-gimbal CMGs. When designing ISS reaction control, a system was required to be capable of maintaining stability during assembly, mating, and robotic arm operations, among other dynamic operations. Several disadvantages associated with thruster reaction control prevented their selection for primary ISS attitude control: copious use of propellant, contamination of solar arrays, and stress applied to the ISS structure by large moments [7]. CMGs were selected instead as they require only battery power to operate and they can store a large amount of angular momentum within the spacecraft to be applied with a correspondingly large range of control torques. Since their implementation at the ISS, CMGs have provided stability during dynamic operations involving variable and uncertain structural flexibility and mass properties [8]. Included in this list of operations are missions that required large stacks to be stabilized, as when the Space Shuttle was to be docked to the ISS for Orbiter repairs [9].

For comparison, on-off thrusters typical in reaction control systems produce fixed forces and torques over variable on-times. Aside from the drawbacks associated with the ISS attitude control trade study, pointing precision with thrusters is limited by a deadband arising from minimum torque magnitude and duration. CMGs, by contrast, produce variable torques by gimbaling constant-rate flywheels; small gimbal rates correspond to small torques while large gimbal rates correspond to large torques. In order to provide the most benefit to astronaut maneuvering systems or small spacecraft beyond a traditional thruster reaction control system, CMGs must be capable of providing both small torques necessary for fine control and large torques required for large-magnitude disturbance rejection. Spacecraft with moving parts or astronaut maneuvering units based on NASA's SAFER, for instance, would benefit from the capacity of CMGs to provide stability during dynamic operations that, like ISS operations, involve variable (and often unknown) structure flexibility and mass properties.

For the case of small spacecraft and astronaut maneuvering units, MIT and Draper have identified single-gimbal CMGs (as distinguished from the double-gimbal CMGs as used on the ISS) because of their high output torque, their availability in miniature size, and their quick response times (for a review of different CMG configurations and parametric comparisons of design criteria for single- and double-gimbal CMGs, see Auclair [10][*]). Other internal torqueing devices such as reaction wheels and magnetorquers were not selected due to their reduced capacity as

[*] Aside from recent advances in miniaturization and power reduction of single-gimbal CMGs, the concepts presented in [10] are still applicable today.

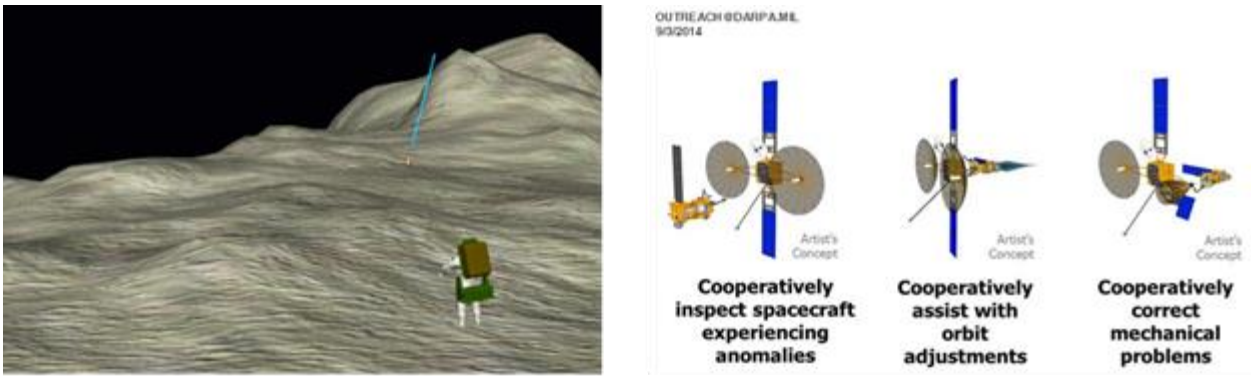

(a) (b)

Figure 1. Mission concepts for CMG and thruster controlled spacecraft. *(a) Draper-MIT advanced Jetpack concept, simulated with human-in-the-loop testing of stability during dynamic operations in collaboration with NASA Johnson Space Center [3]. (b) Servicer or assembly spacecraft, perhaps similar to the DARPA satellite servicer concept, envisioned in the Phoenix program [13].*

compared with single-gimbal CMGs (henceforth referred to simply as CMGs) to deliver large torques and quick response times with small size, weight and power specifications. For a treatment of the topic as applied to small Earth-observing satellites, see Votel [11].

A similar investigation was conducted by NASA in the late 1960s to identify the utility of CMGs in an astronaut mobility unit that would become the Manned Maneuvering Unit (MMU). An integrated demonstration at Skylab was even conducted in 1974 as part of the M509 experiment [12]. Ultimately, however, the high cost and large power and weight of CMGs at the time contributed to their exclusion to the final MMU design despite the increased stability and fuel savings demonstrated at Skylab. With recent miniaturization of CMG and spacecraft technology, this investigation once again becomes highly relevant.

B. Mission Concepts

Missions that stand to gain most from CMG augmented servicers or astronaut maneuvering units include exploration missions to low gravity objects such as Near Earth Asteroids, Martian moons, as well as EVAs in the vicinity of Orion, NASA's next crewed vehicle. It must be noted here that an added urgency for EVA mobility technologies comes from the fact that Orion currently has no provisions for a robotic arm akin to that used at the ISS or on the Shuttle in the past that could help provide a flexible platform for EVA missions. A thruster-based astronaut maneuvering system would be capable of providing mobility to astronauts or robots conducting EVAs, and CMGs added to the system would provide enhanced stability for precision tasks with the extra benefit of conserving fuel.

Figure 1a shows a screenshot of the Draper-MIT Mobility Augmenting Jetpack with Integrated CMGs (MAJIC) human-operated simulation, developed in conjunction with NASA's Johnson Space Center. These simulations and human-in-the-loop studies in which participants actively moved their limbs with simulated tools revealed that CMGs provide a higher level of stability as compared with thrusters for dynamic motions [1, 3-4]. Just as the ISS or an astronaut maneuvering system must provide stability during dynamic motions involving variable mass properties and structural flexibility, so too will future satellite servicer and assembly spacecraft. Current concepts such as that envisioned by the DARPA Phoenix program [13] depicted in Figure 1b do not include CMGs at the moment, though perhaps with more information concerning the utility of small CMGs this may change.

C. Hardware Demonstration with MIT SPHERES

In addition to low gravity astronaut Jetpack design studies for CMG actuator sizing [1-2] and human-in-the-loop simulation [3-4], a hardware demonstration of miniature CMG control for astronaut maneuvering units and small spacecraft has been conducted in MIT's Space Systems Laboratory and aboard NASA's Reduced Gravity Aircraft (RGA) [1, 6]. Demonstrations have employed the MIT Synchronized Position Hold Engage and Reorient Experimental Satellite (SPHERES) facility and a suite of CMGs acquired from Honeybee Robotics, Ltd. (Honeybee). The latest flight campaign complements laboratory experiments conducted in the MIT Space Systems Laboratory (SSL) as well as experimental work completed in a previous flight campaign to test a suite of inspection sensors integrated along with CMGs on the SPHERES platform, described in Sternberg [6].

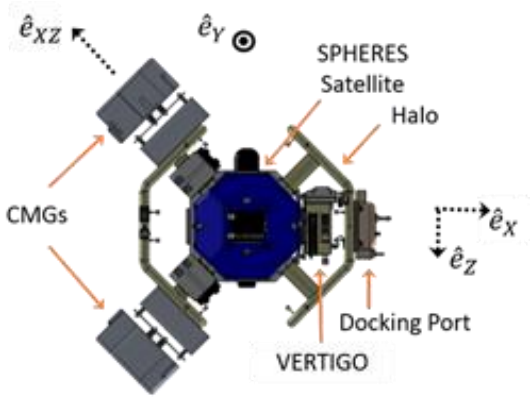

Figure 2. SPHERES satellite configuration. *A central SPHERES satellite with built-in cold gas thrusters is integrated with a Halo expansion. A VERTIGO avionics stack that interfaces with the SPHERES satellite is used to process controls for peripherals such as CMGs and a docking port. SPHERES body frame axes as used in the present experiment are labeled.*

The SPHERES facility is composed of three satellites aboard the ISS and two more in the MIT SSL; each satellite contains 12 cold gas thrusters, an inertial measurement system, communication system, and re-programmable avionics for control algorithm research and development. Recent hardware expansions to the SPHERES facility allow for a single SPHERES satellite to interface with up to six peripheral sensors or actuators through a so-called Halo structure. These expansions have enabled the implementation of an on-off thruster and CMG testbed.

A diagram of the SPHERES system used for thruster and CMG testing is shown in Figure 2. A central Blue SPHERES satellite is depicted, along with an external computer (VERTIGO) that is used to command the CMGs through an electrical connection provided by the Halo expansion ring. The SPHERES coordinate frame used in the experiment is also depicted. The docking port shown can be used to mechanically mate the configuration shown with another SPHERES configuration; docking ports are employed in on-going SPHERES research to investigate autonomous docking in the context of reconfigurable spacecraft and service and assembly robotic missions [14], akin to the DARPA Phoenix concept shown in Figure 1b. While the docking port is not used in the current study, future CMG and thruster control experiments are expected to take advantage of the large number of configurations and mission types the expandable SPHERES facility provides.

II. Experiment Design

The set of experiments lying at the center of this discussion involves the comparison of torques delivered to the SPHERES system depicted in Figure 2 first with SPHERES thruster pairs and second with a pair of Honeybee CMGs operating in a scissor pair configuration. Figure 3 depicts a cartoon graphic that illustrates the difference between the two types of actuation. For both microgravity and laboratory experiments, actuation times of one second (1 s) along a torque vector τ_i (where *i* labels the SPHERES-frame axis) are applied, followed by a 0.5 s pause. Next a torque of the same magnitude but opposite sign, $-\tau_i$, is applied for 1 s followed by another 0.5 s pause. This sequence is repeated until a command to cease the test is given to the SPHERES satellite. On-board inertial measurement gyroscopes are used to record angular rates that, when combined with information about the satellite's mass properties, can then be converted into torque measurements.

Satellite mass properties can alternatively be identified from computer-aided design (CAD) models, or from open loop torque experiments with known torques. The identification of SPHERES mass properties from open loop torques is accomplished by using characterized SPHERES thruster pairs to produce a well-defined average torque on the system. For more information, please see Section IV. Estimation of Torques from Measured Angular Rates, below.

A. Thruster Pair and CMG Physics

Before introducing thruster or CMG physics, the governing rotational equation of motion for a spacecraft (s/c) should be introduced as [15]

$$\vec{\tau}_{\mathrm{s/c}} = I\dot{\vec{\omega}}^{B/N} + (\vec{\omega}^{B/N} \times I\vec{\omega}^{B/N}) \tag{1}$$

where $\vec{\tau}_{s/c}$ is the torque on a spacecraft, I is the mass moment of inertia tensor of the spacecraft with respect to the center of mass and $\vec{\omega}^{B/N}$ is the angular rate vector of the spacecraft body frame B with respect to the inertial frame N. Thrusters and CMGs are two actuators that can induce torques $\vec{\tau}_{s/c}$ on the system. Thruster pair torques $\vec{\tau}_{thr}$ and CMG subsystem torques $\vec{\tau}_{CMG\ total}$ will be considered individually.

A single thruster's actuation produces a torque $\vec{\tau}_{1\ thr}$ on the spacecraft if the thrust vector is not aligned with the spacecraft center of mass but instead acts with a moment arm $\vec{r}$. The force of a thruster $\vec{F}_{thr}$ is the product of the mean propellant exit velocity $\vec{v}_{prop}$ and mass flow rate $\dot{m}$ according to the usual relation $\vec{F}_{thr} = -\dot{m}\vec{v}_{prop}$. The torque $\vec{\tau}_{thr\,1}$ this single thruster's force generates at a moment arm $\vec{r}$ is given by

$$\vec{\tau}_{thr\,1} = \left(\vec{F}_{thr} \times \vec{r}\right)\sin\xi = \left(-\dot{m}\vec{v}_{prop} \times \vec{r}\right)\sin\xi \tag{2}$$

In order to produce a pure torque without an associated force applied to the spacecraft, the moment arm $\vec{r}$ should be orthogonal to the thrust vector $\vec{F}_{thr}$, or equivalently, orthogonal to the propellant exit velocity $\vec{v}_{prop}$. The $\sin\xi$ term in Equation 2 accounts for misalignments of the thrust vector angle from perpendicular. A thruster pair involves the firing of two thrusters oriented opposite one another across the spacecraft center of mass, each providing a torque to the system, as depicted graphically in Figure 3a. A thruster pair-induced torque $\vec{\tau}_{thr}$ is equal to twice the torque of the single thruster at a moment arm $\vec{r}$ as:

$$\vec{\tau}_{thr} = 2\left(\vec{F}_{thr} \times \vec{r}\right)\sin\xi = 2\left(-\dot{m}\vec{v}_{prop} \times \vec{r}\right)\sin\xi \tag{3}$$

A time-integration of Equation 3 yields the angular momentum $\vec{L}_{thr}$ that is added to the system over the time period T of torque actuation with a thruster pair:

$$\vec{L}_{thr} = 2\left(\vec{F}_{thr}T \times \vec{r}\right)\sin\xi = 2(-m\vec{v}_{prop} \times \vec{r})\sin\xi \tag{4}$$

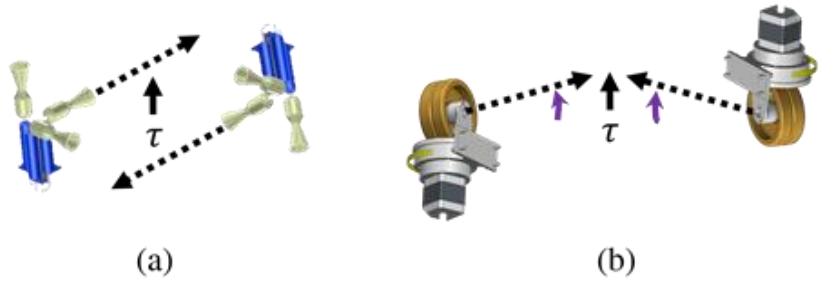

Figure 3. Thruster pair and CMG scissor pair executing a torque. *(a) Thruster pairs fire in opposite directions (dotted arrows) to produce a torque (solid arrow). (b) CMG torque along a single axis (solid arrow) is achieved with a scissor pair by gimbaling opposing flywheel angular momentum vectors (dotted arrows) such that their collective angular momentum is always aligned in a single axis (the torque axis).*

While thrusters produce torques by firing opposing thrusters simultaneously, a single CMG produces torque by gimbaling a fixed-rate flywheel. An expression for the torque on a spacecraft $\vec{\tau}_{CMG\ total}$ induced by a suite of CMGs with collective angular momentum H_{CMG} is given by [16]

$$\vec{\tau}_{CMG\ total} = \dot{\vec{H}}_{CMG} + \vec{\omega}^{B/N} \times \vec{H}_{CMG} \tag{5}$$

where the magnitude $\vec{\omega}^{B/N}$ is the same angular rate of the spacecraft body frame B with respect to the inertial frame N as in Equation 1. Equation 5 is simply the sum of time-varying CMG angular momentum and a dynamic cross-coupling of CMG momentum with rotation of the spacecraft. $\vec{H}_{CMG}$ is composed of the sum of all individual CMG momenta ($\vec{H}_{CMG} = \sum \vec{h}_{CMG}$); embedded within each actuator's momentum $\vec{h}_{CMG}$ are the (dominant) flywheel angular momentum $\vec{h}_{fly}$ and minor contributions from CMG gimbal structure.

If two CMGs are configured in a so-called scissor pair configuration as depicted in Figure 3b, then their gimbal axes are parallel and the CMGs are positioned such that their flywheel angular momentum vectors point at one another and cancel, leading to a collective $\vec{H}_{CMG} = 0$. In this orientation, gimbal angles ϕ_1 and ϕ_2 are defined to be null. When performing a torque, commanded gimbal rates $\dot{\phi}_1$ and $\dot{\phi}_2$ (and thus gimbal angles ϕ_1 and ϕ_2 for the two CMGs) are constrained to be equal and opposite, and the vector sum $\vec{H}_{CMG}$ becomes non-zero. The collective angular momentum for a scissor pair is then expressed as [12, 17]

$$\vec{H}_{CMG} = 2\,|\vec{h}_{CMG}|\sin\phi\ \hat{e}_i \tag{6}$$

In Equation 6 the $\sin\phi$ term derives from the fact that angular momentum only constructively adds along the $\hat{e}_i$ torque axis when gimbal angles $\phi_1 = -\phi_2 \equiv \phi$ deviate from $\phi = 0$, with a maximum collective angular momentum achieved when $\phi = \pi/2$. The total scissor pair torque $\vec{\tau}_{CMG\,sp}$ is found by combining Equations 5 and 6; for simplicity, let us assume that initially the spacecraft has no rotational velocity in the inertial frame and also that the spacecraft moment of inertia *I* is diagonal; in this case dynamic cross-coupling is eliminated and the scissor pair torque can be expressed simply as [12, 17]

$$\vec{\tau}_{CMG\,sp} = -2\,h_{CMG}\,\dot{\phi}\cos\phi\,\hat{e}_i \approx -2\,h_{fly}\,\dot{\phi}\cos\phi\ \hat{e}_i \tag{7}$$

The negative sign in Equation 7 is included to emphasize the fact that torques generated by CMGs produce an equal and opposite torque on the spacecraft. The torques for each individual CMG are aligned along $\hat{h}_{CMG} \times \hat{\phi}$, but only constructively sum along the vector $\hat{e}_i$; the $\cos\phi$ term reflects the contributions to torque that cancel. For this reason, the vector magnitudes for angular momentum and gimbal rate are used in Equation 7 as opposed to their vector forms. Furthermore, because flywheel angular momentum dominates, the approximation $h_{CMG} \approx h_{fly}$ can be made as indicated by the right-most expression.

Note that while CMG momentum (Equation 6) is maximized at $\phi = \pi/2$, CMG torque is maximized at $\phi = 0$. Should the gimbal angle reach $\phi = \pi/2$, no further torque can be applied in this direction and saturation occurs. In order to continue applying torques in the same direction, an external torque is required to bring the CMGs back to a position in which they once again have control authority. This is accomplished, for instance, with thrusters or as in the case with the ISS, with a gravity gradient (for more information on CMG configurations and associated desaturation algorithms, see Jones, Zeledon and Peck [17] or Kirokawa [18]).

B. Comparison of Reaction Control Deadbands

The introduction of the physics of thruster and CMG reaction control motivates a comparison of control deadbands. A deadband is usually defined as the uncontrollable region in angular space, $\Delta\Theta$, that characterizes the precision limit for pointing (a 2° deadband corresponds to $\Delta\Theta = \pm 1°$). In addition to pointing, a reaction control system is often charged with controlling the slew rate and the angular acceleration of a spacecraft. These objectives, too, have associated deadbands, or unavoidable absolute errors, that correspond to the smallest increment in slew rate $\Delta\Omega$ and angular acceleration ΔA.

Unavoidable absolute errors in pointing or slewing arise from a non-zero minimum *torque impulse*, a term defined here to be the product of an actuator's torque and actuation time, or the angular momentum generated by a torque of a given duration. Of course, if the resolution of inertial sensors is sufficiently coarse, sensor uncertainty (as opposed to minimum torque impulse) can drive the size of a deadband. This is a trivial case for the purposes of control theory and will not be discussed further in this paper.

For each on-off thruster pair, thrust cannot be modulated and thus nominal torque from a firing event is constant. Torque impulse is minimized only through on-times. Equation 8 is an expression for minimum thruster pair torque impulse:

$$\vec{L}_{SPH\,thr,min} = 2\left(\vec{F}_{thr}T_{thr,min} \times \vec{r}\right) = 0.3\hat{e}_i \text{ mN m s} \tag{8}$$

The SPHERES' thrusters have a nominal thrust magnitude $|\vec{F}_{thr}| =$ 0.1 N, a moment arm $r = 10$ cm and minimum on-time of $T_{thr,min} = 15$ ms. $\vec{F}_{thr}$ was characterized by Chen [19] from 3- and 6-degrees-of-freedom experimental data with the assumption of orthogonality between thrust vector and moment arm, hence it already embeds a misalignment sine factor. Equation 8 is evaluated with these constants to yield a minimum torque impulse of $\vec{L}_{SPH\,thr,min} = 0.3$ mN m s directed along the torque axis $\hat{e}_i$.

CMGs differ from thruster pairs as reaction control actuators in that CMGs can modulate both their output torque magnitude and duration. The minimum torque impulse for this study is calculated by applying the minimum gimbal rate $\dot{\phi}_{min} = 0.011$ rad s^{-1} to the two CMGs of a scissor pair for the minimum actuation time $T_{CMG,min} = 10$ ms. In this case, the change in gimbal angle from the initial $\phi = 0$ is on the order of 1e-4 and so the loss term $\cos\phi = 1$. Using these values along with the nominal flywheel angular momentum magnitude $|\vec{h}_{fly}| = h_{fly} = 108$ mN m s, the minimum CMG torque impulse is calculated to be:

$$\vec{L}_{CMG,min} = \int_0^{T_{CMG,min}} -2h_{fly}\dot{\phi}_{min}\cos\phi\,\hat{e}_i\,dt = 0.02\hat{e}_i \text{ mN m s} \tag{9}$$

Note that the gimbal angle $\phi = \dot{\phi}T$ is time-dependent. A quick comparison of the right hand sides of Equations 8 and 9 reveals that a Honeybee CMG scissor pair can provide torque impulses that are an order of magnitude smaller than the minimum possible torque impulse for the thruster pair. With smaller torque impulses, CMGs have the potential to control the SPHERES to a more precise degree.

The direct observation of smaller torques imparted to the SPHERES satellites with CMGs as compared with thrusters is one objective for experimentation; a second and corresponding objective is to observe larger torques with CMGs to demonstrate their potential to quickly reject larger disturbance torques than thrusters can reject on the SPHERES platform.

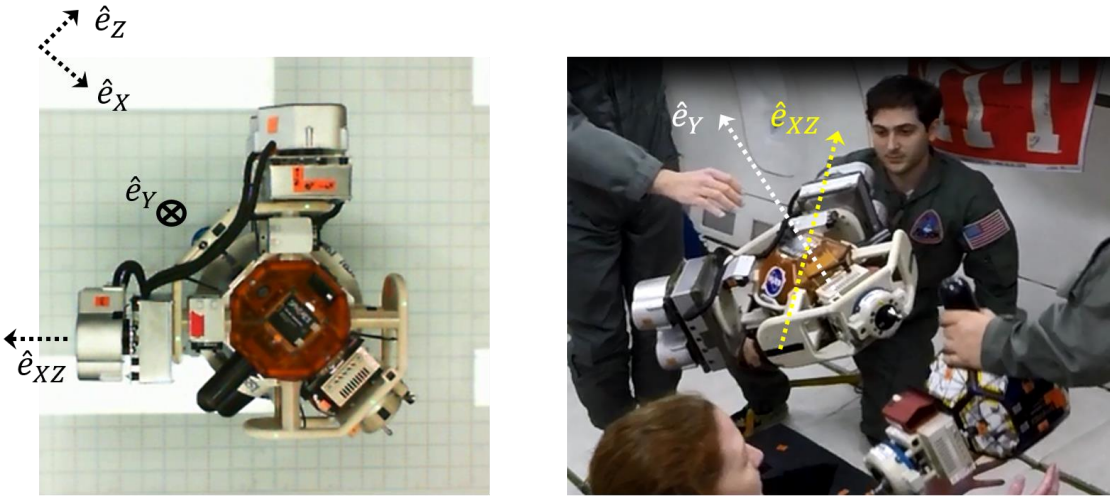

Figure 4. Experiment photographs. *Laboratory tests (a) and microgravity tests (b) with NASA's Reduced Gravity Aircraft; experiments are designed to investigate the utility of CMGs as attitude actuators for the SPHERES facility and astronaut mobility units derived from NASA's SAFER..*

C. Lab and Reduced Gravity (RG) Coordinate Frames

In the laboratory, scissor pair torques and thruster torques are applied in the SPHERES principal y-axis $\hat{e}_Y$ while on parabolic flights torques were applied along multiple SPHERES axes. Unfortunately, problems with CMG hardware during the microgravity flight campaign restricted usable open loop torque data for CMGs to the SPHERES $\hat{e}_{XZ} = -(\hat{e}_X + \hat{e}_Z)/\sqrt{2}$ axis, where $\hat{e}_X$ and $\hat{e}_Z$ are the SPHERES x- and z- principal axes, respectively as shown in Figure 4. Unlike the principal axes, the $\hat{e}_{XZ}$ does not have a single thruster pair aligned in order to provide a pure torque; instead torques along this axis are executed by simultaneously firing both x- and z- axis thruster pairs. Figure 4a shows a photograph of the SPHERES apparatus as viewed in the MIT laboratory floating on a glass table. Figure 4b shows a photograph of the free-floating apparatus in NASA's Reduced Gravity Aircraft. In both photographs, relevant axes are labeled.

D. Selection of Open Loop Torques

SPHERES thruster-induced torques have fixed magnitude, and so appropriate thruster on-times must be selected such that observable angular rates are produced. In the laboratory this is a simple matter of extending torque times, but in parabolic flight experiments useable microgravity windows are often shorter than expected due to turbulence or an imperfect parabolic trajectory.[†] In order to ensure maximum useful data collection for microgravity flights, torque durations must be sufficiently long such that SPHERES inertial measurement gyros can reliably measure accrued angular rates (measurement requirement). In addition to this requirement, when conducting experiments on board the Reduced Gravity Aircraft, torque times must be limited in order to allow for multiple actuations in a single reduced gravity parabola (repeatability requirement).

Finally, there is an added benefit to limiting the duration of torque times: for CMGs, sustained torques eventually saturate the scissor pair configuration, and for thrusters, sustained firings reduce the consistency of thrust magnitude (constant actuation requirement). A constant actuation requirement of one second (1 s) was determined to sufficiently enable both CMGs and thrusters to produce reliable and repeatable control. The SPHERES gyro has a minimum resolution of 7.1×10^{-4} rad/s, meaning angular rates of at least 7.1×10^{-3} rad/s (10x larger than sensor resolution) were identified as necessary for statistically significant measurements. By using CAD models for the SPHERES configuration to be used in microgravity and a 1 s actuation time, the minimum torque to be tested was calculated to be 5 mN m.

In order to satisfy the repeatability requirement, tests are designed to execute open loop torques along a given axis first in one direction, followed by a brief (0.5 s) pause, followed by an actuation in the opposite direction. Substantive data sets were collected despite the uncertainty and time limitations inherent to parabolic flights by using automated torque cycles. In order to most readily compare results from microgravity with those from the laboratory, the same open torque actuation cycle (1 s of actuation in one direction followed by a 0.5 s pause, followed by 1 s of actuation in the opposite direction) is used.

For CMGs, initial torque magnitudes (hereafter referred to as commanded torques) are selected to be: 5 mN m, 10 mN m, 20 mN m, 40 mN m, 100 mN m and 200 mN m. These torque magnitudes correspond to the initial torque the CMG pair provides. Over the course of a 1s actuation time, the total torque impulses that would be produced from constant torque are simply 5 mN m s, 10 mN m s, 20 mN m s, 40 mN m s, 100 mN m s and 200 mN m s; however, if constant gimbal rates are used instead, the actual torque impulses produced will be somewhat less than these values because of the $\cos\phi$ loss term in Equation 7. For instance, for a scissor pair torque in the SPHERES-y axis, the integral $\int_0^1 \vec{\tau}_{CMG\ sp}\, \hat{e}_Y\, dt = \int_0^1 -2h_{fly}\dot{\phi}\cos\phi\, \hat{e}_Y\, dt$ is evaluated for each initial torque, yielding (in units of mN m s directed along $\hat{e}_Y$): 5.00, 10.00, 19.97, 39.77, 96.47, and 172.62.

Table 1 shows the different actuator torques that are selected for experimentation. The SPHERES coordinate frame introduced above (Section II. C. Lab and Reduced Gravity Coordinate Frames) is indicated by subscripts. Note that

Table 1. Actuator torques selected for experiment.

Actuator	SPHERES Thrusters (Principal Pairs)	SPHERES Thrusters (Diagonal XZ Pair)	Honeybee H120 CMG Scissor Pair					
Nominal Torque	$\lvert\vec{\tau}_{thr}\rvert = \tau_X = \tau_Y = \tau_Z =$ 20 mN m	$\lvert\vec{\tau}_{thr}\rvert = \lvert\vec{\tau}_{XZ}\rvert$ $\sqrt{2}(\tau_X + \tau_Z) =$ 28.3 mN m	$\lvert\vec{\tau}_{CMG\ sp}\rvert = \lvert\vec{\tau}_{XZ}\rvert = \lvert\vec{\tau}_Y\rvert$ (mN m)					
			5	10	20	40	100	200
			% torque impulse reduction ($\cos\phi$ loss from Eq. 7) for 1s torque					
			0.01	0.04	0.14	0.57	3.5	14

[†] Each parabola affords on average ~15 s of microgravity, though with a large free-floating apparatus like the SPHERES configuration shown in Figure 4, the average undisturbed free-floating time we observed was < 5 s.

for CMG torques, the loss factor over an actuation of 1s (attributable to the $\cos\phi$ term from Equation 7) is indicated below each initial torque value. This torque impulse reduction is insignificant until high torques are performed (3.5% loss for 100 mN m initial torque and 14% reduction for 200 mN m initial torque). In future experiments that aim to characterize CMG torques with high fidelity, these losses will play a significant factor. In the present study, which aims to demonstrate that CMGs provide a range of torques that span the torque attainable with the SPHERES thruster pair, these losses are not as important to consider. For low torques the loss factor is negligible and for high torques there is no question that CMGs can produce higher SPHERES angular accelerations than thruster pairs; losses in high torques simply contribute to uncertainty in CMG torque characterization, a topic on which future research will concentrate.

III. Laboratory and Reduced Gravity Aircraft Data

SPHERES inertial measurement sensors record angular rate profiles during open loop torque actuation. For a given experiment either in the laboratory or on NASA's Reduced Gravity Aircraft, periods of time during which the apparatus is undisturbed and actuators are properly functioning are identified with video footage and corresponding measured angular rates are isolated. For each actuation period, a maximum angular acceleration is identified from finite differences of angular rate measurements. Averages of these maxima are then calculated.

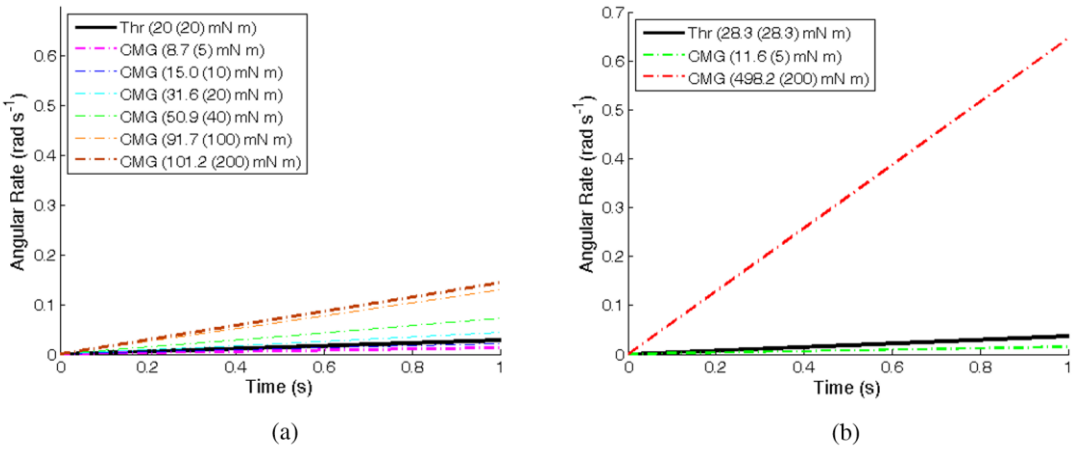

Figure 5. Angular rates vs time. *(a) Laboratory data; (b) Microgravity data. Angular rates observed for multiple experimental trials are averaged and displayed over the actuation time of 1 s. Thruster pair actuation is plotted in solid black ("Thr") while CMG actuation is denoted with dotted lines; line slopes indicate observed angular acceleration. Legend labels follow the format: Actuator (Observed torque (Commanded torque) mN m), where "Thr" stands for thrusters.*

Figure 5 depicts angular rate versus time with slopes corresponding to average angular acceleration maxima. Figure 5a depicts laboratory data while Figure 5b depicts microgravity data. CMG data is plotted with dotted lines while thruster data is plotted as a solid black line. The legends of Figure 5 indicate the actuator type as well as the observed vs. commanded torque corresponding to each time-averaged line. Note that more experimental data was collected for laboratory tests (Figure 5a) given the fact that laboratory testing is free from the time and situational constraints involved with microgravity testing.

A comparison of the y-axes of Figures 5a (laboratory results) and 5b (microgravity results) indicates that similar actuation results in larger angular rates for the microgravity experiments. This result can be attributed to the fact that the ground laboratory set-up involves an air-bearing assembly to float the SPHERES apparatus. This air-bearing assembly increases the mass moment of inertia of the system, contributing to a reduced angular acceleration in Figure 5a arising from the same torque application. In addition, the air-bearing does not provide perfect, friction-less support for the SPHERES assembly and so the extra friction also contributes to a reduced angular acceleration observed in Figure 5a. A better characterization of the air-bearing assembly mass properties will be the subject of future research, as will the investigation of discrepancies observed between expected and observed angular acceleration profiles.

Perhaps the most important feature to identify from both Figure 5a and Figure 5b in the context of the current research objective is that the dotted lines corresponding to CMG actuation have both smaller and larger slopes (i.e.

angular acceleration) than black lines corresponding to thruster-induced actuation. This is important from a controls perspective for two reasons. First, a smaller angular acceleration indicates that a smaller deadband can be afforded and thus a higher degree of pointing precision can be delivered (see above, Section II. B. Comparison of Reaction Control Deadbands). Second, a larger angular acceleration indicates that the SPHERES system using CMGs for reaction control can stabilize a structure with greater torque requirements, either arising from a large moment of inertia or large disturbance torques, than a thruster reaction control system can stabilize.

IV. Estimation of Torques from Measured Angular Rates

In order to draw conclusions about torques provided to the system, the SPHERES system mass moment of inertia about the torque axis *I* must be known in addition to the angular accelerations $\dot{\vec{\omega}}_i^{\,B/N}$ measured from a fixed-SPHERES reference body frame *B* with respect to a laboratory inertial reference frame *N* along the axis $\hat{e}_i$. Note that this angular acceleration is calculated from finite differences of inertial measurement gyroscope angular rate measurements. Torque estimates are constructed by assuming that no dynamic cross-coupling occurs and so angular accelerations directly couple to the system's mass moment of inertia tensor element I_{ii} along the torque axis $\hat{e}_i$:

$$\vec{\tau}_i = I_{ii}\,\dot{\vec{\omega}}_i^{\,B/N}\hat{e}_i \tag{10}$$

For this experiment, cross-coupling dynamic products are an order of magnitude smaller than torques measured according to Equation 10, and so the relation is a valid approximation.

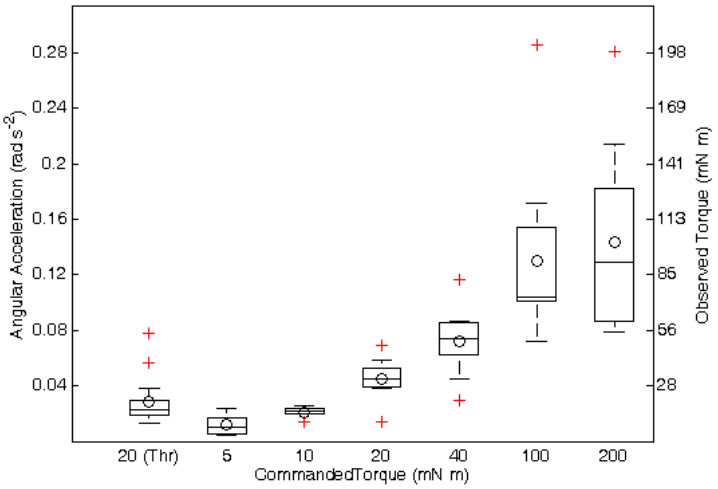

Figure 6. Laboratory observed torque vs. commanded torque. *Statistical box plot for thruster pair actuation and CMG scissor pair actuation. Boxes are described by 25%, 50% (median), and 75% quantiles. Circles denote arithmetic means and red crosses denote data points that lie outside ± 2.7σ.*

There are two methods by which a mass moment of inertia can be determined: first, with a computer-aided design (CAD) model, and second, with an experiment utilizing known torques. In the ground laboratory experiments, only the latter method is available since the air-bearing fixtures are not accurately modeled at present (future research will aim to address this). Deriving torques from open-loop experiments using a known torque is accomplished by using SPHERES thrusters, which have been characterized by Chen [19]. Each thruster provides an average of 0.1 N of force per thruster. When using 0.1 N of force in Equation 3, a thruster-torque of 20 mN m results for y-axis torques. Measurements for angular acceleration observed during laboratory open loop thruster torques τ_Y are then used to derive a mass moment of inertia I_{YY} using Equation 10. This moment of inertia is then in turn used to calculate torques produced by CMGs (which have not yet been fully characterized) through multiplication with observed angular acceleration (again, Equation 10).

Figure 6 depicts a statistical box plot of inertial measurements for open loop ground laboratory experiments; both thrusters and a range of commanded CMG torques are depicted. Boxes feature 25%, 50% (median), and 75% quantiles to indicate variance of data. Circles denote arithmetic means and red crosses denote data points that lie outside ± 2.7σ where σ is one standard deviation. The data plotted corresponds to angular rate finite differences (i.e. angular acceleration measurements) indicated in the left-hand y-axis. Corresponding torques calculated using known thruster torques are shown in the right-hand y-axis.

Figure 7 displays data from microgravity experiments in the same manner as Figure 6. That is, a statistical box plot is used to display angular acceleration data collected, and torques are calculated with a mass moment of inertia derived from known, open-loop thruster firings. Figure 7a depicts thruster data alongside minimum and maximum

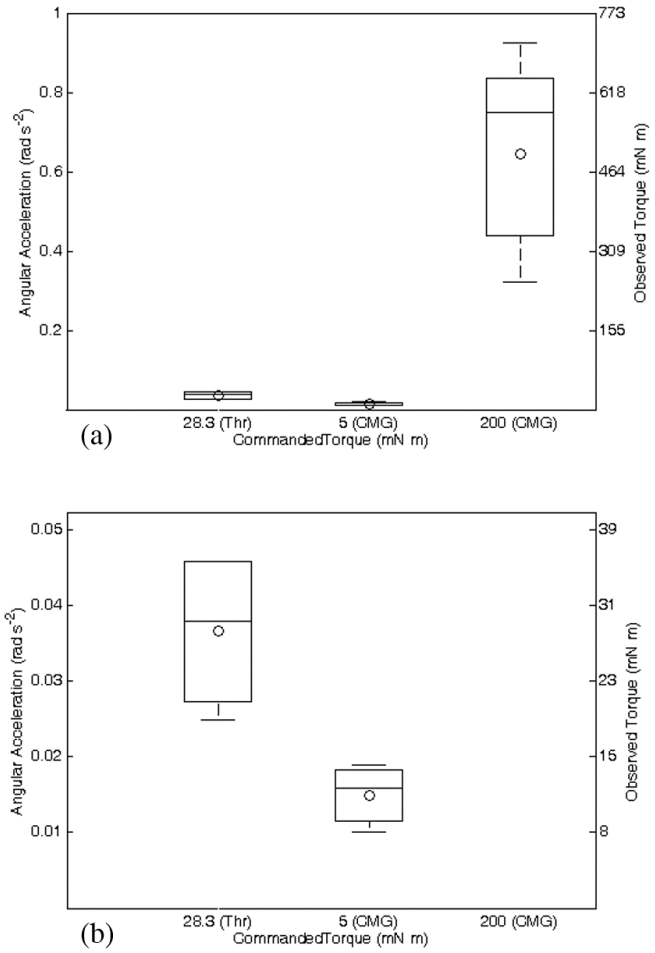

Figure 7. Microgravity observed torque vs. commanded torque.
(a) Statistical box plot for thruster pair actuation and CMG scissor pair actuation in the SPH-XZ axis. Boxes are described by 25%, 50% (median), and 75% quantiles, and circles denote arithmetic means. (b) Zoomed perspective of XZ thruster actuation (nominal 28.3 mN m) and minimum CMG actuation (5 mN m command).

CMG torques observed on-board the Reduced Gravity Aircraft. Figure 7b shows a zoomed perspective so that the angular acceleration and torque values for thrusters and CMGs can be compared more directly.

The right-hand y-axis of Figure 7a indicates that when commanded to produce 200 mN m of torque, CMGs are observed to generate between 300-600 mN m (as indicated by the box in the "200 (CMG)" column). The source of this discrepancy likely has several sources including uncertainty in CMG characterization as well as potential deviations from the nominal 0.1 N SPHERES thrust during moment of inertia characterization. Due to the fact that CMGs experienced hardware problems leading up to and during flight experiments, the discrepancies in maximum torque observed and maximum torque expected will have to be investigated through further laboratory testing using upgraded hardware. As part of the new series of tests, a simulation of the effects of uncertainties on torques expected will also be considered to help disambiguate similar discrepancies in the future.

It is also interesting to note the relative variance in distributions; large CMG torques have the greatest absolute variation both in microgravity as in the laboratory as can be observed by the box sizes in Figures 6 and 7. But when compared on a percentage scale (i.e. the standard deviation as a percentage of the mean), the actuators perform similarly well. In microgravity, thruster torques and 5 mN m CMG torques both vary by 30% while 200 mN m CMG torques vary by 37%. In laboratory measurements, variations are more pronounced as might be expected from the added uncertainties associated with friction; CMG torque variations are: 51% for 5 mN m torques, 16% for 10 mN m, 32% for 20 mN m, 34% for 40 mN m, 48% for 100 mN m and 45% for 200 mN m. Thrusters, by contrast, have the largest percentage variation at 62% for laboratory tests.

Without microgravity testing it would appear from laboratory tests alone (and with statistical significance) that thrusters have worse repeatability as evidenced by their large percentage variation. The fact that thrusters and CMGs displayed roughly equivalent percentage variations in microgravity testing reveals that the variation observed in the laboratory was not a feature of thrusters. Instead this observation can be attributed to the uncertainties inherent in ground experiments, which do not enjoy the same advantages that inertial experiments enjoy in microgravity. Even with similar percentage variation, the data collected indicate without doubt that the SPHERES system can be provided with both smaller magnitude and larger magnitude torques when actuated with CMGs as compared as with thrusters for attitude adjustments. This strengthens the argument that CMGs would reduce an effective deadband and improve overall pointing precision in a closed loop control architecture as compared with using thruster pairs as the primary attitude control system for SPHERES configurations.

V. Conclusion

The objective of ground-based and microgravity experiments was to investigate the relative control authority of on-off thrusters and CMGs using the SPHERES platform. This was accomplished by measuring angular rates in open loop experiments. The primary limitation of on-off thrusters is that they provide a single torque magnitude that can be modulated only with variable on-times. This means that a system designed for precision pointing will be ill-equipped to handle large disturbance torques, or conversely, this means that a system designed for fast slews or for the manipulation of large structures with time-varying mass properties will have a reduced capacity for precision pointing.

CMGs, on the other hand, have the capacity to modulate their output torque; in the case of the SPHERES system tested in microgravity and in the laboratory, CMGs have demonstrated both smaller and larger torques as evidenced by data depicted graphically in Figures 5-7. Future research will aim to better characterize CMGs with a specific emphasis on resolving the apparent disconnect between commanded torques and observed torques.

Of course, in addition to providing a wider range of control torques for improved stability, CMGs have the added benefit that they are propellantless actuators; their use, then, implies fuel savings as well as a reduction in potential contamination of surfaces in the vicinity of reaction control thrusters. The drawback of using CMG is the extra weight, cost and complexity required to include them in a spacecraft system. The relative benefits of improved stability and fuel economy must be weighed against these disadvantages on a case-by-case basis. Because CMGs can saturate, external torqueing means are necessary to ensure sustained, successful operations. In small systems like the ones considered in this research, thrusters most readily provide this external torque since they are most likely incorporated into the system already as actuators to provide positional control.

Based on the results obtained in this research in addition to the findings of previous studies at MIT and Draper [1-6], miniature CMGs can be regarded as a capable means to provide a large range of torques for the purposes of improved stability; this utility is most readily applicable to astronaut mobility units and spacecraft with variable mass or flexural properties as with assembly and servicing spacecraft. With upgraded Honeybee CMGs to operate with full rotational control, the SPHERES facility will soon be poised to build upon the demonstrations described in this paper in order to explore closed-loop architectures that make full use of the advantages of CMGs.

Acknowledgments

The authors of this paper would like to thank the Charles Stark Draper Laboratory Inc. for their support in hardware efforts that were necessary to realize these experiments. We would also like to acknowledge the NASA Reduced Gravity Office for their support, which enabled us to conduct tests in microgravity aboard their Reduced Gravity Aircraft.

References

[1]Sheerin, T. F., "Design and Utility Assessment of Attitude Control Systems for EVA Task Performance*," Master's Thesis*, MIT Aeronautics and Astronautics, Cambridge, MA. August 2015.

[2]Sheerin, T. F., Carpenter, M. D., Hoffman, J. H., "Actuator Sizing and Utility Assessment of Control Moment Gyroscopes for an Astronaut EVA Jetpack," *Proceedings of the 45th International Conference on Environmental Systems*, Bellevue, WA. July 2015.

[3]Carpenter, M. D., Jackson, K. F., Cohanim, B. E., Duda, K. R., Dopart, C. H., Rize, J. P., Sheerin, T. F., and Hoffman, J. A., "Operator Evaluation of a Mobility-Augmenting Jetpack with Integrated Control-Moment Gyroscopes," *Proceedings of the 36th IEEE Aerospace Conference*, Big Sky, MT, March 2015.

[4]Dopart, C. H., "Astronaut-Centric Analysis of a Jetpack with Integrated Control-Moment Gyroscopes for Enhanced Extravehicular Activity Performance*," Master's Thesis*, MIT Aeronautics and Astronautics, Cambridge, MA. May 2014.

[5]Carpenter, D. M., Jackson, K., Cohanim, B., Duda, K. R., Rize, J., Dopart, C., Hoffman, J. A., Curiel, P., Studak, J., Poncia, D., and Zumbado, J. R., "Next-Generation Maneuvering System with Control-Moment Gyroscopes for Extravehicular Activities Near Low-Gravity Objects," *Proceedings of the 43rd International Conference on Environmental Systems*, Vail, CO. 14-18 July 2013.

[6]Sternberg, D., Sheerin, T. F., and Urbain, G., "INSPECT Sensor Suite for On-Orbit Inspection and Characterization with Extravehicular Activity Spacecraft." *Proceedings of the 45th International Conference on Environmental Systems*, Bellevue, WA, July 2015.

[7]Bedrossian, N. S., Bhatt, S., Kang, W., Ross, M., "Zero-Propellant Maneuver Guidance: Rotating the International Space Station with Computational Dynamic Optimization," *IEEE Control Systems Magazine*, pp. 53-73, October 2009.

[8]Bedrossian, N. S., "International Space Station Assembly and Operational Control Challenges," *Proceedings of the 23rd Guidance and Control Conference*, Breckenridge, CO, February 2000.

[9]Bedrossian, N. S., Jang, J-W., Alaniz, A., Johnson, M., Sebelius, K., Mesfin, Y., "International Space Station US GN&C Attitude Hold Controller Design for Orbiter Repair Maneuver," *Proceedings of the AIAA Guidance, Navigation and Control Conference and Exhibit*, San Francisco, CA, August 2005.

[10]Auclair, G. F., Wells, R. C. "Control Moment Gyro Selection and Design Criteria," *Proceedings of the AIAA Guidance, Control and Flight Mechanics Conference*, Santa Barbara, CA. 17-19 August, 1970.

[11]Votel, R., Sinclair, D., "Comparison of Control Moment Gyros and Reaction Wheels for Small Earth-Observing Satellites," *Proceedings of the 26th AIAA/USU Conference on Small Satellites*, Logan, UT. 2012.

[12]Murtagh, T. B., Whitsett, C. E., Goodwin, M. A., and Greenlee J. E., "Automatic Control of the Skylab Astronaut Maneuvering Research Vehicle," *Journal of Spacecraft, 11(5): 321-326 May 1974.*

[13]Defense Advanced Research Projects Agency, Phoenix Program, *http://www.darpa.mil/news-events/2014-09-03*.

[14]Sternberg, D., Miller, D., Jewison, C., James, J., Hilton, A., McCarthy, B., Roascio, D., Saenz-Otero, A., "Reconfigurable Ground and Flight Testing Facility for Robotic Servicing, Capture, and Assembly," *Proceedings of the 37th IEEE Aerospace Conference*, Big Sky, MT, March 2016.

[15]Meirovitch, L., *Methods of Analytical Dynamics*, McGraw-Hill, New York, 1970, Ch. 4.

[16]Cramer, P. S. and Josephson, J. T., "ASMU Attitude Control System Design: M509 Experiment," Rept. MCR-29-486, prepared under Contract NAS9-0339, Aug. 1969, Martin Marietta, Denver Division, Denver, CO.

[17]Jones, L. L., Zeledon, R. A., and Peck , M. A., "Generalized Framework for Linearly Constrained Control Moment Gyro Steering," *Journal of Guidance, Control, and Dynamics*, 35(4): 1094-1103, 2012.

[18]Kurokawa, H. "Survey of Theory and Steering Laws of Single-Gimbal Control Moment Gyros." *Journal of Guidance, Control, and Dynamics*, 30(5): 1331-1340, 2007.

[19]Chen, A., "Propulsion System Characterization for the SPHERES Formation Flight and Docking Testbed*," Master's Thesis*, MIT Aeronautics and Astronautics, Cambridge, MA. May 2002.